Spatio-Temporal Analysis of Epidemic Development of Leather Rot of Strawberry

K. M. Reynolds, L. V. Madden, and M. A. Ellis

Postdoctoral research associate and associate professors, respectively, The Ohio State University (OSU) and Ohio Agricultural Research and Development Center (OARDC), Wooster 44691.

Salaries and research support provided by State and Federal funds (especially USDA Competitive Grant 85-CRCR-1-1537) appropriated to OARDC-OSU, Journal Article 36-87.

Accepted for publication 13 July 1987 (submitted for electronic processing).

ABSTRACT

Reynolds, K. M., Madden, L. V., and Ellis, M. A. 1988. Spatio-temporal analysis of epidemic development of leather rot of strawberry. Phytopathology 78:246-252.

The temporal and spatial patterns of strawberry leather rot, caused by *Phytophthora cactorum*, were monitored in three field plots near Wooster, OH, from 15 May to 15 June 1986. Each plot was 2 m in length, three rows wide, and partitioned into 60 quadrats (10 20-cm-long quadrats on each side of a crop row). Straw mulch was removed from the two interior aisles, but left on the two exterior sides. Plots were infested on 15 May with strawberry fruit on which *P. cactorum* was sporulating. Assessments of disease incidence in each quadrat were made by counting the number of cymes bearing at least one infected fruit. By 8 June, disease incidence was $> 60\%$ in all but two of the interior sides but $< 10\%$ in the exterior sides. Data were analyzed using the spatio-temporal (ST) autocorrelation analysis program, STAUTO, to identify the appropriate temporal and spatial lag orders for specification of model parameters in ST autoregressive moving average (STARMA) models. When spatial autocorrelations and partial spatial autocorrelations of disease incidence between quadrats were calculated for each plot over the 10 rain events, first-, second-, and third-order spatial autocorrelations exhibited clear positive trends in each plot, indicating that disease incidence within neighboring quadrats at a given time was becoming progressively similar as the epidemic developed. No such trends were apparent in the partial autocorrelations. The first-order spatial partial autocorrelation was significant in all three plots for the last six rain events, whereas higher-order partial autocorrelations never attained significance in any plot, indicating a lack of spatial dependence between disease incidence in quadrats beyond the first spatial lag at any given time. Analyses of separate across- and within row-side ST autocorrelations of disease incidence demonstrated that a strong barrier effect was operating across crop rows. The highest levels of ST autocorrelation for all three plots were observed using the rook's definition of spatial proximity and a crop row barrier specification that was obtained by trial and error. Initial model identification was based on the use of temporally differenced data, since analysis of the raw data and ST autocorrelograms indicated that the data were nonstationary over time. Interpretation of ST autocorrelograms and partial ST autocorrelograms suggested that the ST transfer functions that generated the observed patterns of fruit infection in plots 3 and 6 were very similar, and that change in the logit of disease incidence within a quadrat could be predicted in terms of the mean change and a single disturbance (error) term. However, the ST transfer function in plot 2 was best represented by either a STIMA(1, 1) or a STARIMA(1, 1, 1, 1) model. Differences in model forms required to represent the epidemic processes in the three plots appeared to be the result of differences in topographic and edaphic factors that affected splash dispersal of the pathogen.

Quantitative analysis of epidemics began in earnest with the now classic temporal models of Vanderplank (21), whose methods treated epidemic development as a homogeneous spatial process. However, plant pathologists recently have also demonstrated considerable interest in describing the spatial patterns of disease (3,10,14). Descriptive statistics such as the variance-to-mean ratio (5), Lloyd's indices of mean crowding and patchiness (9,20), and the negative binomial k parameter (15) have proven useful in characterizing the spatial association of diseased plants. Interpretations of the epidemic process based on these point pattern statistics can be employed to infer certain basic characteristics of an epidemic such as mean patch size (20) or true versus apparent contagion (4).

A basic characteristic of all point pattern statistics is that they only describe a spatial pattern at a single point in time. Thus, these analyses provide only very general insights into the evolutionary process that led to the state of the system at the time of disease assessment. Spatial autocorrelation measures are similarly limited. Madden et al (11) have shown that the utility of spatial autocorrelation methods can be extended by examining how these statistics change over time. However, the approach of Madden et al (11) is still not sufficient for the identification and specification of models that describe how such patterns evolve through time.

Spatio-temporal (ST) autocorrelation analysis is a relatively new analytical method that can be applied to the analysis of epidemics when data are collected from repeated observations over time and from a lattice (regular rectangular grid) of contiguous quadrats. In contrast to analytical methods cited above, ST autocorrelation analysis can be used for identification of the spatio-temporal transfer function (STF) that describes the development of an epidemic in time and space (1,2,4,12,16,18). An STF is an empirical function that describes the temporal and spatial relationship between the values associated with the elements that compose the lattice (e.g., disease observations), and the function is typically composed of autoregressive and moving average terms that may be lagged both in time and space. The principal feature distinguishing this method from others is that temporal and spatial characteristics of a process are analyzed

simultaneously (2). Reynolds and Madden (18) have summarized the central theoretical developments of ST autocorrelation analysis, and an exhaustive treatment of the theory can be found in Bennett (2).

In this study, the methods of ST autocorrelation analysis were used to identify the STF of the epidemic process operating in the case of leather rot of strawberry (*Fragaria* × *ananassa* Duch. 'Midway'), caused by *Phytophthora cactorum* (Leb. & Cohn) Schroet., which has been shown to be splash dispersed (6,17,19). The goal of our analytical procedure was to identify the appropriate model order, within the general model class known as spatio-temporal autoregressive moving average (STARMA) models, needed to describe the splash dispersal of *P. cactorum* in time and space.

MATERIALS AND METHODS

Plot establishment. Six plots were established in a commercial strawberry field near Wooster, OH, in early May 1986 before flowering. Each plot was 2 m long and three crop rows wide. The straw mulch was removed from the center aisles of plots 2, 3, and 6. Because of lack of disease development in the other three plots, only data from plots 2, 3, and 6 were used in the present study. Five flower cymes closest to the row aisle were tagged in each of 10 20-cm-long sections on each side of a crop row, providing a lattice of 6 by 10 quadrats in each plot. For the purposes of subsequent discussion, the six crop-row-sides of a plot will hereafter be referred to as sides 1–6, with sides 1 and 6 being the two external sides of a plot. Note that sides 2 and 3 as well as sides 4 and 5 are pairs (pairs 2-3 and 4-5, respectively) in which the members of each pair face one another across a crop row aisle. Similarly, in the pairs of sides, 1-2, 3-4, and 5-6, the members of each pair are adjacent, but on opposite sides of the same crop row.

Plot infestation and disease assessment. Infected strawberry fruit were prepared by the method of Grove et al (7), and each plot was infested with fruit on which *P. cactorum* was actively sporulating. Five infected fruit were placed at the southern edge of each plot between pairs 2-3 and 4-5 on 15 May (inoculum was placed at the ends of plots rather than the middle to provide maximum distance for disease movement). Disease assessments were performed 5 days (maximum length of latent period under ambient weather conditions) after each of 10 rain events during the period 15 May to 10 June (Fig. 1). At each assessment, disease incidence (DI) was assessed as the number of tagged cymes in a quadrat that bore one or more infected fruit.

Statistical analysis. It is important to understand that, although most of our graphical results are presented in terms of chronological time, for purposes of analysis, the units of "time" are rain events (e.g., time is measured in events, not hours or days). Events were used as the unit of time rather than chronological time, since spread of *P. cactorum* between fruit is known to occur only by rain splash. Thus, for practical purposes, chronological time is not particularly relevant.

Lloyd's index of patchiness of DI was computed for each plot at each sample date (9). Spatial autocorrelations and partial spatial autocorrelations were also calculated for each sample date using logit(DI), binary distance weighting, and the rook's definition of spatial proximity (18).

A preliminary ST analysis was performed using quadrat observations transformed to logit(DI), and in which ST autocorrelograms for three spatial (s) and three temporal (k) lags were generated for separate across- and within-side neighbor effects for each plot, using binary distance weighting (4,18,20). The latter analysis was performed to assess whether or not differences existed between autocorrelations within sides and autocorrelations across sides. The strengths of crop row barrier effects were subsequently determined by trial and error as that set of barrier specifications yielding the largest improvement in across-side autocorrelations (18).

Autocorrelograms for nondifferenced, logit-transformed data were generated using the barrier specification set obtained above, and using three alternative spatial proximity patterns (rook, queen, and square) and two alternative distance weighting criteria (binary and inverse distance). Autocorrelograms produced by the alternative proximity patterns and weighting criteria were compared to determine which combination produced the highest general level of ST autocorrelation and to check for evidence of spatial and/or temporal nonstationarity in each data set (2,18).

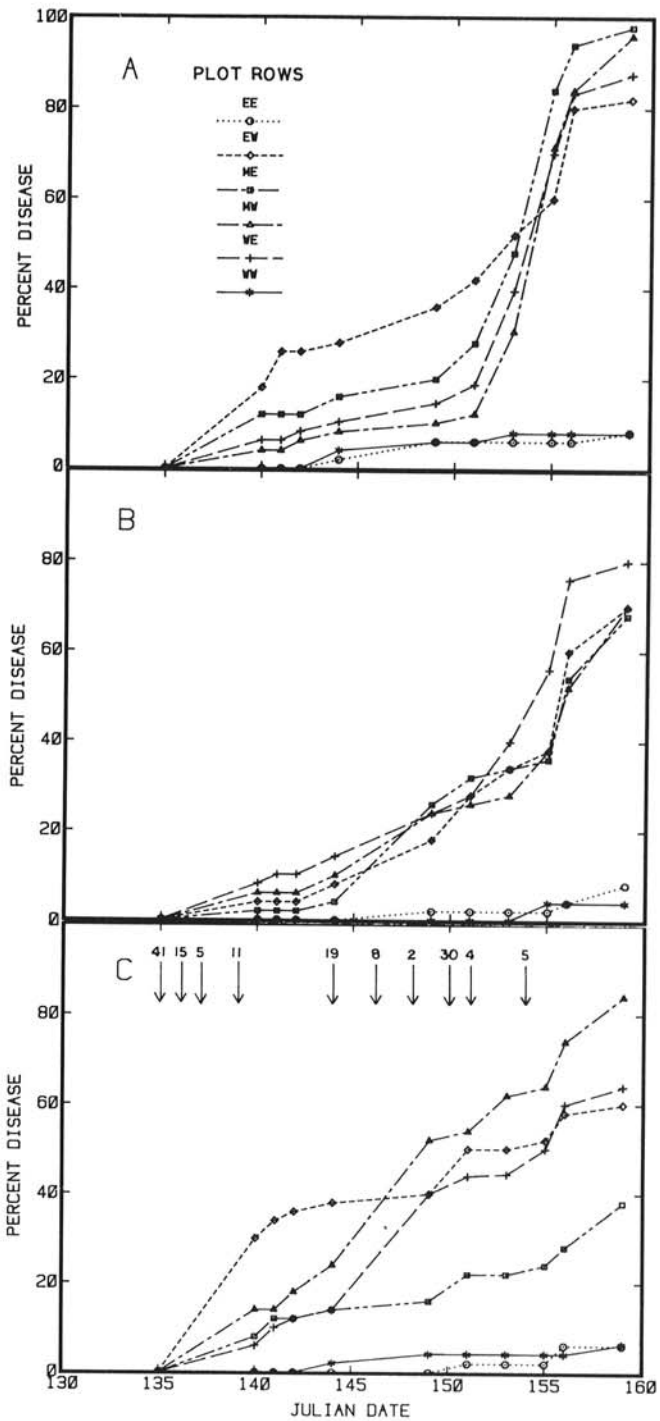

Fig. 1. Progress of leather rot development in field plots from 15 May (day of the year [Julian date] = 135) to 9 June (day of the year = 159) 1986. Straw mulch was removed from the interior aisles, but left on the external sides of each plot. Disease incidence in the figure is summarized as percent of strawberry cymes bearing at least one infected fruit on each side of each of three rows per plot (plot length was 2 m). The six sides of rows are designated by plot position (panel A): side 1 was the west side of the west row (WW), and side 6 was the east side of the east row (EE). Arrows (panel C) indicate approximate time of rain events, and numbers over arrows indicate rainfall amount in millimeters. Disease assessments were performed 5 days after each rain event. **A,** Plot 2. **B,** Plot 3. **C,** Plot 6.

Initial model identification was based on z statistics of the autocorrelations and partial autocorrelations and the general patterns observed in the autocorrelograms and partial autocorrelograms (1,2,11,15,18).

Parameter estimation for the general class of STARMA model is accomplished by conditional maximum likelihood estimation (CMLE, 16). The method is quite complex, and not generally available, although we are working on an adaption of the algorithm of Pfeifer and Deutsch (16). Because of the current lack of suitable CMLE procedure, initial model specification was only possible for the simplest cases analyzed in this study. A companion program to STAUTO also was developed for use in verification of STARMA models (STVER). STVER uses a model specified by the analyst, together with a set of initial lattice values, to compute predicted values for the spatio-temporal data series. The program outputs residuals for subsequent analysis via STAUTO. Like STAUTO, STVER allows for the specification of proximity patterns, distance weighting, and barrier effects. In the present study, STVER was used to obtain the residuals, and these were then analyzed in STAUTO to check for patterns in the residuals that would indicate an underspecified model (e.g., a model from which significant moving average or autoregressive terms had been omitted).

RESULTS

Disease progress within sides 2–5 in each plot generally exhibited a pattern typical of logistic increase, whereas disease development within sides 1 and 6 was very limited (Fig. 1). Trends in Lloyd's index of patchiness over the 10 assessment dates were very similar in plots 2 and 3 (Fig. 2). In both plots, DI patterns determined at each of the first five assessments (day of year 140–149) were generally uniform to slightly underdispersed (< 1). Between assessments 6 and 10 (day of year 151–159), the index of patchiness in plots 2 and 3 exhibited a slight but fairly consistent positive trend, with final values for patchiness being 1.10 and 1.15 for plots 2 and 3, respectively (Fig. 2). The latter trend in plots 2 and 3 indicates a slight tendency toward aggregation late in the epidemic (e.g., after day of year 155).

The trend in Lloyd's index for plot 6 was markedly different from that observed for plots 2 and 3. In plot 6, index values were quite large for days 140–144, indicating an initially high degree of disease aggregation (Fig. 2). However, the index for plot 6 declined steadily over the sequence of rain events so that, by the last assessment date, Lloyd's index for plot 6 was nearly identical to that for plots 2 and 3.

Consistent positive trends over time in first-, second-, and third-order spatial autocorrelations were observed in each plot, indicating that logit(DI) within neighboring quadrats was becoming progressively similar over time (Fig. 3A). Although there were no significant autocorrelations before the seventh assessment (day of year 153), first-order autocorrelations for plot 6 were much greater than those for plots 2 and 3. First-order spatial autocorrelations were significant in all three plots for the last four assessment dates (days 153–159, Fig. 3A). Similarly, first-order partial spatial autocorrelations were significant in each plot for the last six assessment dates (days 149–159) and also tended to increase over time (Fig. 3B). However, temporal trends in higher-order spatial partial autocorrelations were much less apparent or entirely lacking, and generally not significant (Fig. 3B). The absence of significant higher-order partial spatial autocorrelations indicates that spatial autocorrelations for $s > 1$ were a consequence of collinearity in the lattice observations, so that significant dependence between values of logit(DI) among lattice elements did not extend beyond one spatial lag in any rain event.

ST autocorrelations were significantly greater for within- than for across-side neighbors, when these statistics were calculated separately (Table 1). Thus, logit(DI) within the side of a row appeared to be much more strongly affected by the prior level of logit(DI) within quadrats belonging to the same side of a row than by the prior level of logit(DI) within quadrats belonging to different row-sides, indicating that crop rows were acting as barriers to splash dispersal of *P. cactorum*. The barrier specification set yielding the greatest increase in across-side autocorrelations was [0.1, 1.0, 0.5, 1.0, 0.1] for row-sides 1-2, 2-3, and so on (Table 2).

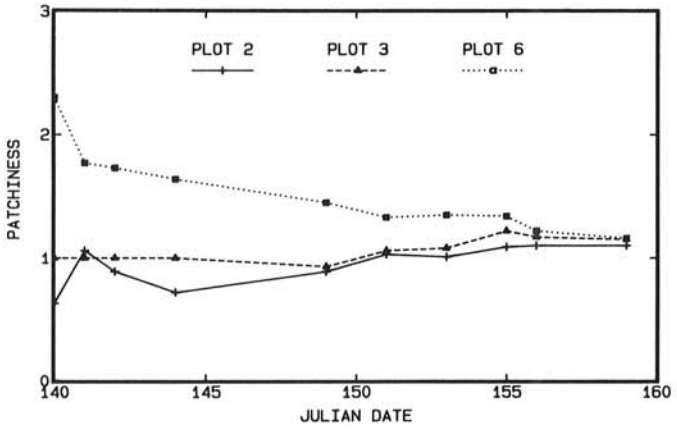

Fig. 2. Patterns of leather rot aggregation assessed over 10 rain events using Lloyd's index of patchiness (9,20).

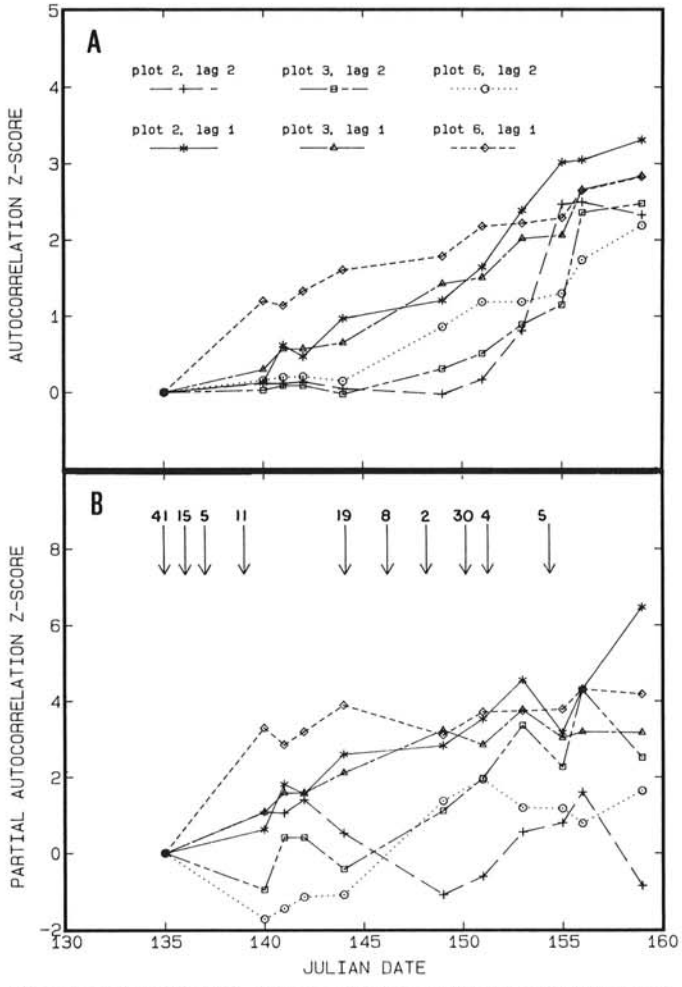

Fig. 3. Z-statistics for first- and second-order spatial autocorrelations and partial autocorrelations of disease incidence among lattice elements for leather rot development in field plots. All estimates were calculated for nondifferenced, logit-transformed values of disease incidence, using the rook's definition of spatial proximity and binary distance weights. Arrows (panel B) indicate approximate time of rain events, and numbers over arrows indicate rainfall amount in millimeters. **A,** Spatial autocorrelations. **B,** Partial spatial autocorrelations.

TABLE 1. Within- and across-row spatio-temporal autocorrelations between leather rot incidence on strawberry cymes and spatially and temporally lagged incidence values[a]

Temporal lag order	Across-row autocorrelations[b] Spatial lag order 0	1	2	3	Within-row autocorrelations[b] Spatial lag order 0	1	2	3
Plot 2								
1	0.88***	0.36***	0.25**	0.02	0.88***	0.79***	0.73***	0.73***
2	0.68***	0.21*	0.17	−0.02	0.68***	0.62***	0.55***	0.57***
3	0.40***	0.00	0.03	−0.06	0.40***	0.37***	0.29**	0.33***
Plot 3								
1	0.88***	0.18*	0.24**	0.10	0.88***	0.64***	0.74***	0.65***
2	0.73***	0.13	0.15	0.02	0.73***	0.50***	0.62***	0.53***
3	0.55***	0.08	0.07	−0.04	0.55***	0.35***	0.49***	0.41***
Plot 6								
1	0.92***	−0.08	0.00	−0.08	0.92***	0.62***	0.59***	0.56***
2	0.83***	−0.12	−0.03	−0.10	0.83***	0.56***	0.51***	0.52***
3	0.74***	−0.13	−0.05	−0.10	0.74***	0.51***	0.44***	0.48***

[a]The logit transformation was applied to each lattice cell observation prior to analysis, based on a maximum of five possible cyme infections. Binary distance weighting also was used.
[b]*, **, and *** following table values indicate that autocorrelations were significant at $P = 0.05$, $P = 0.01$, and $P = 0.001$, respectively.

TABLE 2. Across-row spatio-temporal autocorrelations between leather rot incidence on strawberry cymes and spatially and temporally lagged incidence values, using the barrier effect specification[a]

Temporal lag order	Across-row autocorrelations[b] Spatial lag order 0	1	2	3
Plot 2				
1	0.88***	0.46***	0.34***	0.27**
2	0.68***	0.31**	0.25**	0.22*
3	0.40***	0.07	0.14	0.17
Plot 3				
1	0.88***	0.24**	0.24**	0.24
2	0.73***	0.16	0.19*	0.19*
3	0.55***	0.09	0.15	0.16
Plot 6				
1	0.92***	0.10	0.12	0.15
2	0.83***	0.04	0.09	0.13
3	0.74***	−0.01	0.07	0.11

[a]The logit transformation was applied to each lattice cell observation before analysis, based on a maximum of five possible cyme infections. Binary distance weighting also was used. The barrier set was (0.1, 1.0, 0.5, 1.0, 0.1).
[b]*, **, and *** following table values indicate that autocorrelations were significant at $P = 0.05$, $P = 0.01$, and $P = 0.001$, respectively.

Among the combinations of spatial proximity pattern and distance weighting, ST autocorrelations were generally higher for each plot when the rook's definition of spatial proximity was used in conjunction with binary distance weighting and the above set of crop row barrier specifications. Example ST autocorrelograms representing each proximity pattern-distance weighting combination are presented for plot 2, whose results are typical of all three plots (Table 3). For the three proximity patterns tested, use of inverse distance weighting consistently resulted in a general reduction in ST autocorrelations in the three plots (Table 3). All combinations of pattern and distance weighting showed strong indications of temporal and spatial nonstationarity as evidenced by the failure of autocorrelations to decay rapidly in time and space, respectively (Table 3). Because the number of spatial and temporal lags was limited, the evidence for nonstationarity seen in the correlograms was not conclusive. However, the disease progress curves for individual sides within each plot showed strong evidence of temporal nonstationarity (Fig. 1). Moreover, examination of logit(DI) values within and across sides over time provided no evidence of spatial nonstationarity. Consequently, temporal differencing of logit(DI) was employed in the final ST autocorrelation analysis in addition to the use of binary distance weighting and barrier effects. The autocorrelograms and partial autocorrelograms were dramatically altered as a result of differencing (Table 4). Results for plots 3 and 6 were quite similar. The lack of any significant autocorrelations or partial autocorrelations for plots 3 and 6 indicated that the STF in both cases might be represented by an extremely simple model whose general form is given by:

$$\nabla_T y_{i,t} = \mu + \xi_{i,t} \tag{1}$$

in which ∇_T is the temporal difference operator, which is given by:

$$\nabla_T y_{i,t} = y_{i,t} - y_{i,t-1} \tag{2}$$

and in which μ is a constant, $\xi_{i,t}$ is normally distributed with mean 0 and variance σ^2, and L^s is the spatial lag operator (18). The maximum likelihood estimate (MLE) of μ is just the grand spatio-temporal mean of the temporal differences of logit(DI), while the MLE of σ^2 is given by the variance of the $\nabla_T y$'s. Substituting and the MLEs of μ for plots 3 and 6 into equation 1 gives, respectively:

$$y_{i,t} = y_{i,t-1} + 0.24 + \hat{\xi}_{i,t}, \quad \hat{\xi}_{i,t} \sim NID(0,0.27) \tag{3}$$

and

$$y_{i,t} = y_{i,t-1} + 0.17 + \hat{\xi}_{i,t}, \quad \hat{\xi}_{i,t} \sim NID(0,0.25) \tag{4}$$

Due to the similarity of the models for plots 3 and 6 (Eqs. 3 and 4, respectively), the μ parameters and the variances of $\xi_{i,t}$ were averaged to obtain a common model for the two plots:

$$\nabla_T y_{i,t} = 0.21 + \hat{\xi}_{i,t}, \quad \hat{\xi}_{i,t} \sim NID(0,0.26) \qquad (5)$$

Results of the model verification procedure using STVER indicated that the model specification (Eq. 5) was incomplete. Although there were no ST autocorrelations that could be considered significant for any temporal lag at a spatial lag greater than 0, ST autocorrelations at $s = 0$ were highly significant for at least the first three temporal lags (Table 5). Only the partial autocorrelation for $s = 0$ and $k = 1$ was considered significant. The patterns observed in both the autocorrelations and partial autocorrelations were suggestive of a pure autoregressive process in the residuals of equation 5 (Table 5). This, in turn, would indicate the need for at least one moving average term with $s = 0$ and $k = 1$ in the original difference equations for plots 3 and 6, since

TABLE 3. Spatio-temporal autocorrelations between leather rot incidence on strawberry cymes and spatially and temporally lagged incidence values for plot 2, using different combinations of spatial proximity pattern and distance weighting criteria[a]

Rook pattern

Temporal lag order	Autocorrelations with binary weighting[b] — Spatial lag order 0	1	2	3	Autocorrelations with inverse distance weighting[b] — Spatial lag order 0	1	2	3
1	0.88***	0.81***	0.74***	0.75***	0.88***	0.81***	0.56***	0.45***
2	0.68***	0.71***	0.66***	0.68***	0.68***	0.71***	0.51***	0.40***
3	0.40***	0.47***	0.49***	0.54***	0.40***	0.47***	0.43**	0.35***

Queen pattern

Temporal lag order	Autocorrelations with binary weighting — Spatial lag order 0	1	2	3	Autocorrelations with inverse distance weighting — Spatial lag order 0	1	2	3
1	0.88***	0.75***	0.65***	0.65***	0.88***	0.75***	0.46***	0.37***
2	0.68***	0.66***	0.59***	0.59***	0.68***	0.66***	0.40***	0.33***
3	0.40***	0.47***	0.49***	0.50***	0.40***	0.47***	0.33**	0.29**

Square pattern

Temporal lag order	Autocorrelations with binary weighting — Spatial lag order 0	1	2	3	Autocorrelations with inverse distance weighting — Spatial lag order 0	1	2	3
1	0.88***	0.75***	0.55***	0.48***	0.88***	0.75***	0.40***	0.31***
2	0.68***	0.66***	0.45***	0.38***	0.68***	0.66***	0.33***	0.28**
3	0.40***	0.47***	0.28**	0.25**	0.40***	0.47***	0.26**	0.24*

[a]The logit transformation was applied to each lattice cell observation before analysis, based on a maximum of five possible cyme infections per quadrat. The barrier specification set (0.1, 1.0, 0.5, 1.0, 0.1) was used in each case.
[b]*, **, and *** following table values indicate that ST autocorrelations were significant at $P = 0.05$, $P = 0.01$, and $P = 0.001$, respectively.

TABLE 4. Spatio-temporal autocorrelations between leather rot incidence on strawberry cymes and spatially and temporally lagged incidence values, using the rook's definition of spatial proximity[a]

Plot 2

Temporal lag order	Autocorrelations[b] — Spatial lag order 0	1	2	3	Partial autocorrelations[b] — Spatial lag order 0	1	2	3
1	0.05	0.28**	0.16	0.20*	−0.07	0.22***	0.07	0.09
2	0.03	0.09	0.05	0.03	−0.05	0.05	−0.03	−0.05
3	−0.05	−0.01	−0.03	−0.02	−0.08	0.01	−0.04	−0.01

Plot 3

Temporal lag order	Autocorrelations — Spatial lag order 0	1	2	3	Partial autocorrelations — Spatial lag order 0	1	2	3
1	−0.01	0.07	0.14	0.13	−0.06	0.03	0.10	0.08
2	0.02	−0.03	−0.02	−0.03	0.01	−0.05	0.00	−0.02
3	−0.05	−0.08	0.06	0.01	−0.03	−0.11*	0.10	0.01

Plot 6

Temporal lag order	Autocorrelations — Spatial lag order 0	1	2	3	Partial autocorrelations — Spatial lag order 0	1	2	3
1	−0.07	0.04	0.06	0.02	−0.11	0.04	0.08	−0.01
2	−0.06	−0.02	−0.05	−0.01	−0.07	0.02	−0.03	0.00
3	−0.06	−0.01	−0.04	−0.03	−0.07	0.04	−0.02	−0.03

[a]The logit transformation was applied to each lattice cell observation before analysis, based on a maximum of five possible cyme infections per quadrat. Binary distance weights and temporal differencing were also used. The barrier specification set (0.1, 1.0, 0.5, 1.0, 0.1) was used in each case.
[b]*, **, and *** following table values indicate that ST autocorrelations were significant at $P = 0.05$, $P = 0.01$, and $P = 0.001$, respectively.

TABLE 5. Spatio-temporal autocorrelations for residuals of leather rot incidence on strawberry cymes using the rook's definition of spatial proximity[a]

Plot 3

Temporal lag order	Autocorrelations[b] Spatial lag order 0	1	2	3	Partial autocorrelations[b] Spatial lag order 0	1	2	3
1	0.81***	0.10	0.19	−0.05	0.61***	−0.03	0.05	0.07
2	0.65***	0.05	0.17	−0.09	0.04	−0.06	−0.07	−0.01
3	0.53***	0.10	0.21	−0.09	−0.01	0.07	0.13*	−0.09

Plot 6

Temporal lag order	Autocorrelations[b] Spatial lag order 0	1	2	3	Partial autocorrelations[b] Spatial lag order 0	1	2	3
1	0.86***	0.22	−0.06	−0.08	0.63***	0.01	0.01	−0.02
2	0.73***	0.16	−0.12	−0.11	−0.00	−0.05	−0.04	−0.01
3	0.64***	0.16	−0.16	−0.10	0.04	0.07	−0.02	0.03

[a]The logit transformation was applied to each lattice cell observation before analysis, based on a maximum of five possible cyme infections per quadrat. Binary distance weights and temporal differencing were also used. The barrier specification set (0.1, 1.0, 0.5, 1.0, 0.1) was used in each case.
[b]*, **, and *** following table values indicate that ST autocorrelations were significant at $P = 0.05$, $P = 0.01$, and $P = 0.001$, respectively.

an autoregressive process in the residuals is equivalent to a moving average process.

The analytical results for plot 2 differ from those described for plots 3 and 6 (Table 4). In particular, the ST autocorrelation and partial autocorrelation for $s = 1$ at $k = 1$ were both clearly significant. Therefore, a likely model form in this case would be either a STIMA(1,1) or STARIMA(1,1,1,1) model (2,11,15,17). Parameter estimation for either model form requires the use of conditional MLE techniques, which are not readily available, but which we plan to develop and present in the near future.

DISCUSSION

The analysis of leather rot development in time and space began with an examination of trends in Lloyd's index of patchiness (Fig. 2) and in spatial autocorrelation coefficients (Fig. 3). Although no significant spatial autocorrelations were observed in any plot before the fifth assessment, it is interesting to note that much higher levels of spatial autocorrelation were obtained for plot 6, and that these initially high autocorrelations corresponded to very high values for Lloyd's index. A correspondence also existed between the trends in Lloyd's index (Fig. 2) and the trends in spatial autocorrelation (Fig. 3). The trends in spatial autocorrelation for plots 2 and 3 were very similar, whereas that for plot 6 was initially quite different. However, the spatial autocorrelations for plot 6 eventually approximated those of plots 2 and 3 (Fig. 3). The same general pattern is also quite apparent for trends in Lloyd's index (Fig. 2).

The analysis of separate within- and across-side ST autocorrelations indicated the presence of a strong barrier effect that operated across crop rows, as evidenced by the much lower ST autocorrelations observed across than within sides (Tables 1 and 2). Because the canopy of a strawberry row is relatively dense, it seemed likely that splash dispersal of *P. cactorum* would be influenced by some form of barrier effect. The barrier specification that was finally selected was arrived at by trial and error, using improvement in the general level of ST autocorrelation as a criterion. In the initial stages of this analysis, we had hoped to be able to deduce an appropriate barrier specification from the data by examining autocorrelations between change in DI in pairs of rows. Unfortunately, the specification of barrier effects derived from such autocorrelations was found to be less than optimal with respect to maximizing across-side ST autocorrelations. It appears that this approach failed as a consequence of aggregating the DI data by the sides of crop rows. Thus, at least for the present, trial and error estimation of barrier effects appears to be the only recourse.

When the ST analysis was performed in both spatial dimensions simultaneously, the highest general levels of ST autocorrelation were observed for the rook proximity pattern. The spatial lag operator (18) for a given lattice element in the rook's case only sums neighbor values that come from lattice elements belonging to the same lattice row or column as lattice element i, whereas the queen and square patterns include additional lattice elements in the spatial lag operator summation (Fig. 1 in 18). Because inclusion of the additional elements almost always resulted in lower ST autocorrelations, these elements may not have represented effective sources of inoculum with respect to disease increase in lattice element i. A possible explanation of the latter observation might be that inoculum dispersal across row barriers is affected by the dispersal path length across a barrier. For instance, when the direction of dispersal is normal to barrier orientation, the path length across the barrier is minimal. As the direction of dispersal becomes more oblique relative to barrier orientation, path length across the barrier increases. Inoculum from element j must travel a greater distance through the plant canopy to reach element i and therefore meets with a larger number of obstacles in the form of plant foliage. Therefore, the strength of a barrier effect across adjacent rows may not be constant, but varies as a function of dispersal path length across a barrier. For the purposes of the present study, we have assumed that barrier effects are, in fact, independent of path length. However, the path length hypothesis deserves further consideration as more data sets become available.

The form of equations 3 and 4 imply that disease in lattice element i increases independently of disease incidence in neighboring lattice elements. Because splash dispersal gradients are generally very steep (12), and that for *P. cactorum* in particular is known to be quite steep (16), the form of equations 3 and 4 might appear to be a very unlikely result. However, both plots 3 and 6 were prone to flooding, as evidenced by the frequent occurrence of standing water after showers of only moderate intensity (< 5 mm hr^{-1}). The accumulation of surface water in these plots may have aided dispersal to such an extent that the relative positions of infested and uninfested lattice elements had little bearing on the ability of one element to supply inoculum to another. In addition, the frequent occurrence of standing water may have given rise to a soil reservoir of inoculum that was well dispersed within these plots, so that each plot effectively had its own supply of inoculum.

The initial specification for plots 3 and 6 only included the term μ (Eqs. 3 and 4, respectively). This model would be designated as STIMA(0, 0), which is the form of a random walk model. However, the verification analysis indicated that equations 3 and 4 were underspecified, and that a moving average process at a spatial lag of $s = 0$ should be included in these models (Table 5). Moving average terms in the general STARMA or STARIMA models are often referred to as error or disturbance terms, and their inclusion in a model is indicative of a significant effect on system behavior due to ignored or unknown external variables (2). It should be

noted that significant moving average effects are indicative of external events that are local in scope. Further model development for leather rot increase in plots 3 and 6 should probably also consider factors such as rainfall amount and other weather variables that influence sporulation of *P. cactorum* and infection of strawberry fruit by the pathogen.

The low level of ST autocorrelations observed for plot 2 after temporal differencing (Table 4) suggests that the STF in this case is not substantially different from that for plots 3 and 6, particularly in view of our earlier position that low values of ST autocorrelation should be evaluated more conservatively when binary weights are used as the distance weighting criterion (18). The factors noted above in connection with the generalized dispersal processes active in plots 3 and 6 were probably also effective to some extent in plot 2. However, the occurrence of non-zero-order autoregressive terms in the model for plot 2 may reflect a real difference between the physical environment of plot 2 and that of plots 3 and 6. Plot 2 was located on a higher and more steeply sloping portion of the field, and consequently was not as prone to flooding. Thus, for plot 2, splash dispersal of *P. cactorum* between lattice elements may have been more dependent on direct dispersal of inoculum from one element to another. Because both the ST autocorrelations and partial autocorrelations at $s = 1$ and $k = 1$ were quite low (Table 4), the generalized dispersal process also appeared to dominate in plot 2.

The analyses of infection incidence pattern development for leather rot began with an analysis of the spatial autocorrelation of disease associated with a sequence of rain events (Fig. 3). If an interpretation of the process underlying pattern development were to be based on the spatial autocorrelations of the latter analysis, one would be led to conclude that the spatial dependence between logit(DI) in lattice elements was extending over time to higher order spatial lags. The partial spatial autocorrelations from the same analysis clearly indicate that spatial dependence never extended beyond a single spatial lag. However, even a consideration of the partial spatial autocorrelations is misleading, since the latter attain very high values, suggesting a strong spatial dependence by the end of the epidemic (Fig. 3). With respect to the processes that generate an observed pattern of disease, the latter analysis is inappropriate and fails, because the temporal dimension is ignored. It is important to note that similarly incorrect inferences will be made when using an ST autocorrelation analysis if the data exhibit nonstationarity, and the nonstationarity is not accounted for by differencing.

Spatio-temporal autocorrelation analysis represents a fundamentally new analytical approach to plant disease epidemiology. Unlike, previous analytical methods, this method allows simultaneous testing of spatial and temporal effects of prior disease history on current epidemic development. The results of our analysis of leather rot epidemiology indicate that the STF may be represented by an extremely simple model structure. Indeed, transformations that effectively linearize the disease progress curve may frequently lead to identification of models similar in structure to a random walk process. The underlying structure of equations 3 and 4 is logistic. It is important to note that departures from the random walk model do not require that we abandon the logistic model as a basis for description of epidemic development. Instead, the basic structure may only require modification by inclusion of additional autoregressive and/or moving average terms. While the logistic model should not be treated as beyond criticism, its applicability to STARMA models that can describe a diversity of epidemics may help to maintain a common theoretical thread through epidemiology. Consequently, it may be possible to reduce the epidemic process to a few simple and fundamental types. Such a result would be in the best spirit of comparative epidemiology (8).

LITERATURE CITED

1. Bennett, R. J. 1975. The representation and identification of spatio-temporal systems: An example of population diffusion in North-West England. Trans. Inst. Br. Geogr. 66:73-94.
2. Bennett, R. J. 1979. Spatial Time Series. Pion Ltd., London. 674 pp.
3. Campbell, C. L., and Noe, J. P. 1985. The spatial analysis of soilborne pathogens and root diseases. Annu. Rev. Phytopathol. 23:129-148.
4. Cliff, A. D., and Ord, J. K. 1981. Spatial Processes: Models and Applications. Pion Ltd., London. 266 pp.
5. Elliot, J. M. 1977. Some Methods for the Statistical Analysis of Samples of Benthic Invertebrates. Freshwater Biol. Assoc. Sci. Pub. No. 25. Ambleside, Cumbria, England. 160 pp.
6. Grove, G. G., Madden, L. V., and Ellis, M. A. 1985. Splash dispersal of *Phytophthora cactorum* from infected strawberry fruit. Phytopathology 75:611-615.
7. Grove, G. G., Madden, L. V., and Ellis, M. A. 1985. Influence of temperature and wetness duration on sporulation of *Phytophthora cactorum* on infected strawberry fruit. Phytopathology 75:700-703.
8. Kranz, J. 1978. Comparative anatomy of epidemics. Pages 34-63 in: Plant Disease, An Advanced Treatise, Vol II: How Disease Develops in Populations. J. G. Horsfall and E. B. Cowling, eds. Academic Press, New York. 436 pp.
9. Lloyd, M. 1967. Mean crowding. J. Anim. Ecol. 36:1-30.
10. Madden, L. V. 1988. Dynamic nature of within-field disease and pathogen distributions. Pages 000-000 in: The Spatial Component of Epidemics. M. J. Jeger, ed. Prentice-Hall, NY. (In press).
11. Madden, L., V., Pirone, T. P., and Raccah, B. 1987. Analysis of spatial patterns of virus-diseased tobacco plants. Phytopathology 77:(in press).
12. Martin, R. L., and Oeppen, J. E. 1975. The identification of regional forecasting models using space-time autocorrelation functions. Trans. Papers Inst. Br. Geogr. 66:95-118.
13. McCartney and Fitt, B. D. L. 1987. Spore dispersal gradients and disease development. Pages 109-118 in: Populations of Plant Pathogens: Their Dynamics and Genetics. W. S. Wolfe and C. E. Caten, eds. Blackwell Scientific Publishers. 280 pp. .
14. Nicot, P. C., Rouse, D. I., and Yandell, B. S. 1984. Comparison of statistical methods for studying spatial patterns of soilborne plant pathogens in the field. Phytopathology 74:1399-1402.
15. Noe, J. P., and Campbell, C. L. 1985. Spatial pattern analysis of plant parasitic nematodes. J. Nematol. 17:86-93.
16. Pfeifer, P. E., and Deutsch, S. J. 1980. A STARIMA model building procedure with application to description and regional forecasting. Trans. Inst. Br. Geogr. 5:330-349.
17. Reynolds, K. M., Bulger, M. A., Madden, L. V., and Ellis, M. A. 1987. New methods using simulated rain to study the splash dispersal of plant pathogens. Phytopathology 77:921-926.
18. Reynolds, K. M., Bulger, M. A., Madden, L. V., and Ellis, M. A. 1988. Analysis of epidemics using spatio-temporal autocorrelation. Phytopathology 78:240-246.
19. Rose, D. H. 1924. Leather rot of strawberries. J. Agric. Res. 28:357-374.
20. Upton, G., and Fingleton, B. 1985. Spatial Data Analysis By Example. John Wiley & Sons, Chichester, England. 410 pp.
21. Vanderplank, J. E. 1963. Plant Diseases: Epidemics and Control. Academic Press, New York. 349 pp.

SUSTAINING ASSOCIATES

ABBOTT LABORATORIES, North Chicago, IL

ADVANCED GENETIC SCIENCES, INC., Oakland, CA

AGRICULTURE CANADA, Vineland Station, Ontario

AGRI-DIAGNOSTICS ASSOCIATES, Cinnaminson, NJ

AGRI-SCIENCES, INC., Long Beach, CA

ALF CHRISTIANSON SEED CO., Mount Vernon, WA

AMERICAN CYANAMID CO.-Agriculture Center, Princeton, NJ

BASF CORPORATION, Parsippany, NJ

BUCKMAN LABORATORIES, Memphis, TN

CALGENE, INC., Davis, CA

CARGILL HYBRID SEEDS, Aurora, IL

CHEVRON CHEMICAL CO., Richmond, CA

CHEVRON CHEMICAL CO., San Francisco, CA

CIBA-GEIGY CORP., Agriculture Division, Greensboro, NC

DEKALB-PFIZER GENETICS, DeKalb, IL

DEL MONTE CORPORATION, San Leandro, CA

DEPARTMENT OF AGRICULTURE-Australia Research Labs, Northfield, S. Australia

E. I. DUPONT DE NEMOURS & CO., INC., Ag. Chem. Dept., Newark, DE

ELI LILLY & CO., Greenfield, IN

FERMENTA PLANT PROTECTION CO., Mentor, OH

FERRY MORSE SEED CO., Modesto, CA

FUNK SEEDS INTERNATIONAL, INC., Bloomington, IL

GREAT LAKES CHEMICAL CORPORATION, West Lafayette, IN

GRIFFIN AG. PRODUCTS CO., Valdosta, GA

GUSTAFSON, INC., Des Moines, IA

HARRIS MORAN SEED CO., Rochester, NY

HARTMAN'S PLANTS, INC., Sebring, FL

H. J. HEINZ CO., Bowling Green, OH

HOECHST ROUSSEL AGRIC. VET CO., Somerville, NJ

ICI AMERICAS, INC., Goldsboro, NC

ILLINOIS CROP IMPROVEMENT ASSOCIATION, Urbana, IL

ILLINOIS FOUNDATIONS SEEDS, INC., Champaign, IL

ISTITUTO DE FITOVIROLOGIA, Torino, Italy

ITESM, Queretaro, Mexico

JANSSEN PHARMACEUTICA, Piscataway, NJ

LOXTON RESEARCH CENTRE, Department of Agriculture, Loxton, S. Australia

MERCK & CO., INC., Rahway, NJ

MILES LABORATORIES, INC., Elkhart, IN

MOBAY CORPORATION, Kansas City, MO

MONSANTO AGRICULTURAL CO., Chesterfield, MO

NOR-AM CHEMICAL CO., Wilmington, DE

NORTHRUP KING CO., Woodland, CA

PENNWALT CORP., Ag. Chem. Div., Philadelphia, PA

PETOSEED CO., INC., Woodland, CA

PIONEER HI-BRED INTERNATIONAL, INC., Johnston, IA

RHONE-POULENC AG. CO., Research Triangle Park, NC

ROHM & HAAS CO., Philadelphia, PA

ROTHAMSTED EXP STATION, Herts, England

SAKATA SEED AMERICA, INC., Salinas, CA

SANDOZ CROP PROTECTION CORP., Des Plaines, IL

O. M. SCOTT & SONS, Marysville, OH

SIERRA CROP PROTECTION CO., St. Louis, MO

UNIROYAL CHEM. CROP PROT. R & D, Bethany, CT

USDA FOREST SERVICE, Forest Pest Management, Ogden, UT

WINDMILL PVT. LTD., Harare, Zimbabwe

W. R. LANDIS ASSOCIATES, INC., Valdosta, GA

W-L RESEARCH, INC., Highland, MD